

A Model for Grain Boundary Thermodynamics

Reza Darvishi Kamachali

Max-Planck-Institut für Eisenforschung, Max-Planck-Str. 1, 40237 Düsseldorf, Germany

Email: kamachali@mpie.de

Abstract: A model is proposed for assessing grain boundary thermodynamic properties based on available bulk thermodynamic data. A relative density field parameter and its gradients are introduced to distinguish and describe the grain boundary region with respect to the corresponding bulk. The Gibbs free energy and the equilibrium phase diagram of grain boundary are derived. Furthermore, grain boundary segregation and the coexistence of the bulk and grain boundary phases in binary alloys are studied. The model is qualitatively demonstrated on segregation and interfacial phase separation in Pt-Au system. Finally, the relationships between the grain boundary density parameter, grain boundary free volume and grain boundary misorientation angle are discussed. The current model is readily applicable to study phase equilibria in grain boundaries and opens possibilities to develop microstructure design concepts based on segregation engineering.

Keywords: Grain Boundary Thermodynamics; Grain Boundary Phase Diagram; Grain Boundary Segregation; Grain Boundary Engineering; Grain Boundary Density.

1. Introduction

Quantitative understanding of the interaction between solute atoms and interfaces is crucial for knowledge-based design and engineering of multicomponent materials. During initial fabrication and/or processing, solute segregation and phase changes at the interfaces greatly influence the functional and structural properties of materials. The simplest type of interfaces is grain boundary (GB) which separates two domains (grains) with the same phase but different crystallographic orientations. GBs are known for their paradoxical role as a source of strengthening [1, 2] and/or weakening [3, 4] in polycrystalline materials. This depends on the structural and chemical properties of GBs and the way they interact with other elements of microstructure, e.g. GB network, secondary-phase particles and mobile defects [5-7]. GB segregation can mediate a whole different sorts of phenomena such as segregation-assisted GB premelting [8], GB transition [9, 10], GB precipitation [11, 12] and GB embrittlement [13-15]. Stabilization of nanocrystalline materials against grain growth [16, 17] is another example where GB segregation can play a critical role.

Segregation to structural defects has been the subject of numerous investigations (see for instance [18-26] and references therein). The studies on interfacial segregation can be traced back to the Gibbs works on interface adsorption [27]. Langmuir [28], McLean [29] and Fowler and Guggenheim [30] have further developed the theory of adsorption for different types of atomic interaction on the surface. Later on, Hart [31, 32] and Guttman [13, 33] extended the theory of adsorption for GBs. Around the same time, in an attempt to describe the critical wetting phenomenon, Cahn has proposed a free energy functional with a nonlocal energy contribution to describe interfacial wetting transitions [34]. Several models since then were developed to study GBs. Ma *et al* [35] proposed a full-field approach for studying GB segregation which describes GB region by the reduced atomic coordination number. Based on the KWC model for GBs [36], Tang *et al* developed a model for order-disorder transitions [37, 38] and phase transition [39] at GBs. Kim *et al* [40] proposed a model for GB segregation based on the equal chemical potential condition [41] between the GB and adjacent bulk. A central aspect of GBs which is considered in all of these models is the non-vanishing gradient terms in composition and structure. Due to this fact, GB phases are also called ‘complexions’ [42-44] to distinguish them from the bulk phase that is supposed to be homogeneous by definition.

Despite the enormous knowledge accumulated over the last century about the fundamental aspects of GBs [25, 26, 45, 46], its application in a technical level is awaiting more comprehensive tools to allow systematic engineering of GBs. In particular, the thermodynamic and kinetic databases of GBs are lagging behind, when compared to the bulk materials, that is mainly due to the intrinsic complexity in the GBs

nature. In fact, even the description of the simplest GB, i.e. a flat GB in a bicrystal, requires determination of eight crystallographic degrees of freedom [45]. Although GB properties are functions of a very large space of variables, one may not neglect the fact that they are made of the same materials as for the grain interior (bulk), albeit deviating in structure and/or composition. Hence, parallel to the novel characterization techniques [47, 48] and automated simulation methods [49, 50] that are increasingly expanding our ability to identify and study GBs and their properties in more details, an alternative approach could be assessing the GB thermodynamics and kinetics based on the thermodynamics and kinetics of their corresponding bulk materials. For this purpose, we need to establish a physical framework that allows an approximation of the GB environment with respect to its corresponding reference bulk material. In the current study, I propose a continuous density field to distinguish and describe the GB region with respect to the corresponding bulk. Based on this idea, (i) the GB's Gibbs free energy is derived and related to the bulk thermodynamic properties, (ii) the equilibrium GB phase diagram is obtained and (iii) the coexistence of the bulk and GB phases is discussed. To demonstrate the application of the current model, GB segregation and interfacial phase separation in Pt-Au system is qualitatively studied. Furthermore, the relationships between the relative density parameter and the GB nature in terms of GB free volume and misorientation angle are discussed. The current density-based model offers a method to assess GB thermodynamics using the available bulk thermodynamic data and it is readily applicable for studying and design of polycrystalline materials as demonstrated in another parallel study [51].

2. A Density-based Model for GB Thermodynamics

In his seminal work, van der Waals proposed that an interface can be described by a continuous density field [52] and its spatial variations. For a GB, that has to accommodate for geometrical mismatch between the adjacent grains, an analogous picture can be portrayed in which the density of the GB will be different than that of the adjacent bulk material. This is, on the one hand, even a simpler case than the van der Waals's setup, because the bulk density on the two sides of the GB are the same. But, on the other hand, it can be more complex because of the crystalline nature of the bulk material that may extend into the GB region. In a first attempt made in the current study, we neglect the heterogeneity of GB density due to the crystallinity (the density variation within the GB plane) and instead focus on the possibility of considering an 'average' relative density parameter and its gradient terms to describe GB. In the following, first the density-based Gibbs free energy of a GB is derived for pure (Sec. 2.1) and binary (Sec. 2.2) systems. Using this free energy description, the equilibrium GB phase diagram (Sec. 3.1) and GB segregation isotherm (Sec. 3.2) are obtained. The model is demonstrated on Pt-Au system. Different aspects of the current model,

in particular the coexistence of the bulk and GB phases and the relationship between the GB density, GB free volume and GB misorientation angle, are discussed in Sec. 4.

2.1 A GB in a pure substance

The Gibbs free energy functional of a system made of a pure substance A can be written as

$$\Phi = \int \frac{G_A}{V_m} dV = \int \rho_m g_A dV \quad (1)$$

where G_A and g_A are the Gibbs energy density per mole and unit mass, respectively. Here V_m is the molar volume and ρ_m is the mass density. By definition,

$$g_A(\rho_m) = E + K + pV - TS \quad (2)$$

where T is temperature, p is pressure, V is volume and E , K and S are potential energy, kinetic energy and entropy per unit mass of the substance A, respectively. Here the potential energy is of particular interest that is a function of the spacing (density) of the atoms. As van der Waals has shown [52] for a heterogeneous system, the potential energy depends on the 'local' density field as well as its 'nonlocal' gradient terms. One can obtain the potential energy density as (see Appendix A for details)

$$E(\rho_m) = -\frac{A}{2}\rho_m - \frac{\kappa}{2}\nabla^2\rho_m \quad (3)$$

where A and κ are the model parameters related to the material properties. In Eq. (3), the higher-order derivatives with respect to ρ_m are neglected. The density field $\rho_m(\vec{r}, t)$ is a local property which is defined per a characteristic volume (see Appendix A for details). Using Eqs. (1)-(3), the Gibbs free energy density (per unit mole) of the system can be written as

$$G_A(\rho) = -\frac{A_A}{2}\rho^2 + (K_A + pV - TS_A)\rho + \frac{\kappa_A}{2}(\nabla\rho)^2 \quad (4)$$

in which $\int (\nabla\rho)^2 dV = -\int \rho \nabla^2 \rho dV$ with $\nabla\rho = 0$ at the boundaries of the integral is used. Since we are interested in the GB density with respect to its corresponding bulk value, a relative (dimensionless) density field $\rho(x) = \frac{\rho_m(x)}{\rho_m^B}$ is used in Eq. (4). Here ρ_m^B is the mass density in the homogeneous bulk phase where $\rho = \rho^B = 1$. In the GB region, $\rho_{GB} \leq \rho < 1$ where we have $\rho = \rho^{GB}$ within the GB central plane.

Furthermore, we obtain $A_A = AV_m\rho_m^B$, $\kappa_A = \kappa V_m\rho_m^B$, $K_A = KV_m\rho_m^B$ and $S_A = SV_m\rho_m^B$. For a complete derivation of Eq. (4) see Appendix A. It is worth noting that in Eq. (4) the local part of the potential energy contains a quadratic term in the density, $-\frac{A_A}{2}\rho^2$, while all other terms have a linear scaling with the density parameter, $(K_A + pV - TS_A)\rho$. This is an important consequence of the current derivation which allows to maintain the continuity of the density profile across a GB, as discussed in the following.

In order to obtain the GB energy, one can compare a heterogeneous system including a GB against a homogeneous bulk system (without a GB) of the same volume that gives

$$G_A^{GB}(\rho) = -\frac{A_A}{2}(\rho^2 - 1) + (K_A + pV - TS_A)(\rho - 1) + \frac{\kappa_A}{2}(\nabla\rho)^2 \quad (5)$$

Inserting Eq. (5) in Eq. (1) and assuming a flat GB centered at position $x = 0$, the equilibrium density profile across the GB will be

$$\rho(x) = \left(\frac{1 + \rho^{GB}}{2}\right) - \left(\frac{1 - \rho^{GB}}{2}\right) \cos\left(\frac{\pi x}{\eta}\right) \quad (6)$$

which satisfies $\frac{\delta G_A^{GB}}{\delta\rho} = 0$ with $\rho(x = 0) = \rho^{GB}$, $\rho(x = \pm\eta) = 1$ and $\frac{\partial\rho}{\partial x}(x = 0) = 0$. Here $2\eta = 2\pi\sqrt{\frac{\kappa_A}{A}}$ is the width of the GB region. See Appendix B for more details on Eq. (6). Figure 1 (a) and (b) show the equilibrium GB density profile. Compared to the current model, the previous phase-field models for GBs such as KWC model [36-39], result in a discontinuous profile of their respective order parameter across the GB, i.e. $\nabla\phi(x = 0) \neq 0$ where ϕ is the corresponding order parameter, as shown in Fig. 1(c) (see also figure 1 in [36, 38] for comparison). The continuity of density profile across GB is also confirmed by atomistic simulations [51]. Having a continuous density profile in the current model allows deriving a GB free energy such that at least for one material point across the GB (at $x = 0$) the gradient energy term $\frac{\kappa_A}{2}(\nabla\rho)^2$ vanishes.

It is also worth noting that in classical phase-field models, such as the multi-phase-field models [53, 54] or solidification model [55], although the interface energy can be finely recovered, a direct description of the gradient energy term in the GB region, which should extend symmetrically with respect to the GB plane, does not exist. The classical phase-field profile across an interface is illustrated in Fig. 1 (c) to compare the different models. In those models, any description of the GB properties is usually defined by introducing an additional function of the order parameter, e.g. $\phi^n(1 - \phi)^n$ with $n \geq 1$, which although will be symmetric still lacks the corresponding symmetry in the gradient energy term. In contrast, the phase-

field crystal models naturally incorporate the local symmetric gradient terms at a GB (see e.g. [56]) that is because of the fourth-order derivative term present in their free energy functional. In fact, the second-order derivative of the density field in the current model (Eq. (3)) resembles the fourth-order derivative term embedded in the phase-field crystal descriptions as $\rho \propto -\nabla\phi$ where ϕ is the order parameter in the classical phase-field description depicted in Fig. 1 (c).

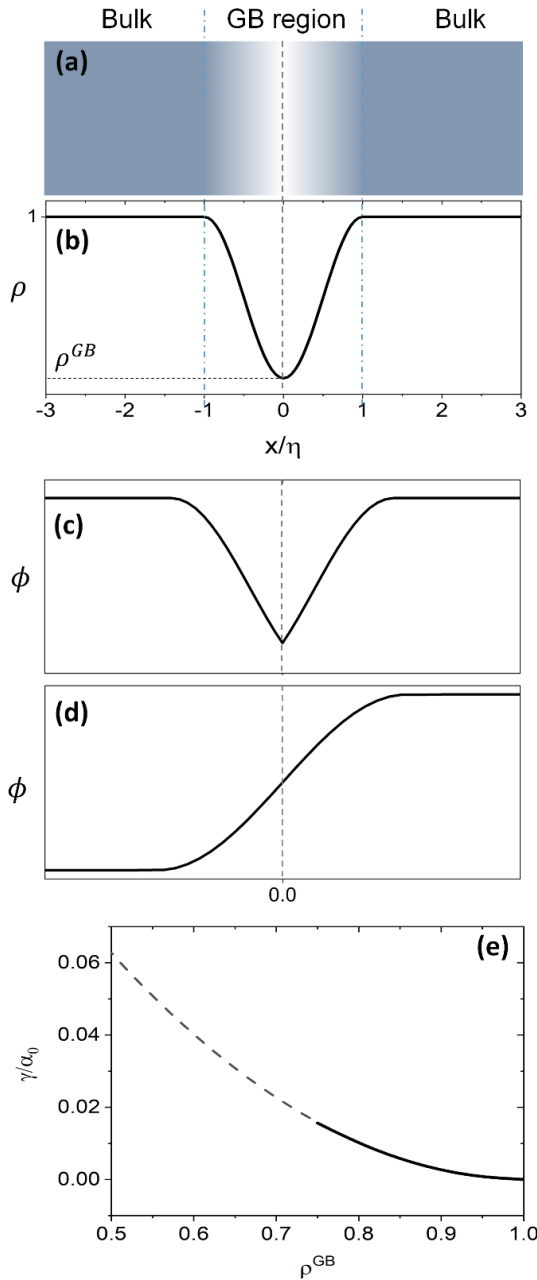


Figure 1: (a) and (b) Continuous density profile across a flat GB with a density $\rho(x = 0) = \rho^{GB}$ is obtained based on the current model (Eq. (6)). The GB width is related to the model parameters A_A and κ_A . The current density profile across GB is compared versus schematic drawing of order parameters from (c) the KWC phase-field model for GBs [36] usually applied for studying GB phase transitions [37-39] and (d) the classical phase-field profile (see for instance [54]). (e) The energy of a flat GB as a function of its density (Eq. (7)) is shown. The solid line indicates the likely range of GB densities (see Sec. 4.2 for discussions).

In the following, ρ^{GB} (the average relative density within the GB plane) will be referred to as ‘GB density’. Using Eqs. (5) and (6) the GB energy $\gamma = 2 \int_0^\eta G_A^{GB} dV$ will be

$$\gamma = \alpha_0 (1 - \rho^{GB})^2 \quad (7)$$

with $\alpha_0 = \frac{\pi}{4} \sqrt{A_A \kappa_A}$. This equation describes the direct relation between GB energy and GB density ρ^{GB} in a pure substance. Figure 1 (e) shows the normalized GB energy $\frac{\gamma}{\alpha_0}$ as a function of ρ^{GB} . The significance of the GB density and its relation with the GB nature is discussed in Sec. 4.2. By applying $\rho = \rho^B = 1$ in Eq. (4) one can recover the bulk Gibbs free energy

$$G_A^B = H_A^B - TS_A^B \quad (8)$$

Here the superscript B indicates the bulk thermodynamic values. For simplifying Eq. (4) we neglect the kinetic energy and pV terms, i.e. $H_A^B \approx -\frac{A_A}{2}$. Thus, Eq. (4) can be rewritten as

$$G_A(\rho) = H_A^B \rho^2 - TS_A^B \rho + \frac{\kappa_A}{2} (\nabla \rho)^2 \quad (9)$$

and consequently, Eq. (5) becomes

$$G_A^{GB}(\rho) = H_A^B (\rho^2 - 1) - TS_A^B (\rho - 1) + \frac{\kappa_A}{2} (\nabla \rho)^2 \quad (10)$$

Equation (9) generalizes the Gibbs free energy description as a function of relative density and relates it to the bulk thermodynamic data.

2.2 GB in a binary alloy

In order to extend the current density-based model for a binary alloy we need to discuss the significance of mixing energy as a function of density parameter. For a bulk regular solution made of A (solvent) and B (solute) atoms, the change in the Gibbs free energy due to the mixing can be approximated [57] as

$$\Delta G_{mix}^B(X_B) = \Delta H_{mix}^B - T\Delta S_{mix}^B = \Omega X_A X_B + RT[X_A \ln X_A + X_B \ln X_B] \quad (11)$$

with

$$\Omega = N_a Z \Delta\epsilon \quad (12)$$

where R is the gas constant, Ω is the mixing enthalpy coefficient, N_a is Avogadro number and Z is the coordination number. $\Delta\epsilon = \left(\epsilon_{AB} - \frac{\epsilon_{AA} + \epsilon_{BB}}{2} \right)$ is bonding energy in which ϵ_{ij} is the bonding energy between atoms i and j and X_A (X_B) is the mole fraction of atoms A (B) with $X_A + X_B = 1$. In principle, the mixing energy terms in Eq. (11) can be assumed to follow the same scaling as found in Eq. (9), i.e. a quadratic ρ^2 proportionality for the enthalpy and a linear ρ proportionality for the entropic contribution. As a matter of fact, the effect of changing the coordination number Z on the GB enthalpy of mixing and GB segregation has been well discussed (see for instance [26, 35, 58] and references therein). While the coordination number is proportional to the local density, the stretch in the bonding energy $\Delta\epsilon$ is also expected to change with the density in the limit of linear elasticity. Considering these facts and neglecting the dependency of configurational entropy for the sake of simplicity, we can write

$$\Delta G_{mix}(X_B, \rho) \approx \rho^2 \Delta H_{mix}^B - T \Delta S_{mix}^B \quad (13)$$

that for $\rho = 1$ returns the bulk mixing free energy Eq. (11). Following Cahn and Hilliard [59] an energy term due to concentration gradient also enters the free energy description. Considering this and using Eqs. (9) and (13) the Gibbs free energy of the regular solid solution (SS) can be written as

$$\begin{aligned} G_{SS}(X_B, \rho) = & X_A \left(H_A^B \rho^2 - T S_A^B \rho + \frac{\kappa_A}{2} (\nabla \rho)^2 \right) + X_B \left(H_B^B \rho^2 - T S_B^B \rho + \frac{\kappa_B}{2} (\nabla \rho)^2 \right) \\ & + \rho^2 \Omega X_A X_B - T \Delta S_{mix}^B + \frac{\kappa_X}{2} (\nabla X_B)^2 \end{aligned} \quad (14)$$

where κ_X is the concentration gradient coefficient. In Eq. (14), corresponding molar fractions X_i^B and X_i^{GB} should be used for the bulk and GB regions, respectively. Again, for the homogeneous bulk material one recovers

$$G_{SS}^B(X_B^B, \rho = 1) = X_A^B (H_A^B - T S_A^B) + X_B^B (H_B^B - T S_B^B) + \Omega X_A^B X_B^B - T \Delta S_{mix}^B \quad (15)$$

Using Eq. (14) we are able now to study the equilibrium GB phase diagram and the coexistence of the bulk and GB phases as presented in the next section.

3. Applications of the Current Density-based Model

3.1 Equilibrium GB phase diagram

From Eq. (14), it is clear that the phase equilibria in a GB region (with $\rho < 1$) should differ from that of the corresponding bulk material. We begin with studying equilibrium phase diagram as the most useful and commonly accepted representation of materials states. Based on the current density-based model, one needs to evaluate the GB phases in equilibrium states by minimizing the Gibbs free energy functional with respect to the concentration and density fields, i.e. $\frac{\delta\Phi}{\delta\rho} = 0$ and $\frac{\delta\Phi}{\delta X_B} = 0$ with $\frac{\delta\Phi}{\delta q} = \frac{\partial\Phi}{\partial q} - \nabla \frac{\partial\Phi}{\partial \nabla q}$ and $\Phi = \int \frac{G_{SS}}{V_m} dV$. Although one can solve these equations numerically and for complex geometries of GBs, the aim of the current study is rather to develop an analytical model for equilibrium GB thermodynamics. A numerical application of the current model will be published elsewhere [51]. Hence a simplified system with a flat GB separating two infinitely large crystals is considered. The GB is centered at $x = 0$ with $\rho(x = 0) = \rho^{GB}$ and $X_B(x = 0) = X_B^{GB}$. As it was discussed in Sec 2.1, the density across the GB is continuous (albeit sharp) with a minimum GB density ρ^{GB} in the center of the GB. Considering the facts that $\nabla\rho(x = 0) = 0$ and $\nabla X_B(x = 0) = 0$ and assuming ρ^{GB} to be a fixed value at equilibrium, the Gibbs free energy description (Eq. (14)) in the center of the GB becomes

$$G_{SS}^{GB}(X_B^{GB}, \rho^{GB}) = X_A^{GB}(H_A^B(\rho^{GB})^2 - TS_A^B(\rho^{GB})) + X_B^{GB}(H_B^B(\rho^{GB})^2 - TS_B^B(\rho^{GB})) + (\rho^{GB})^2 \Omega X_A^{GB} X_B^{GB} - T\Delta S_{mix}^B \quad (16)$$

in which $X_i^{GB} = X_i(x = 0)$. Here the GB density ρ^{GB} represents the nature of the GB and in the following all GB properties correspond to this material point at $x = 0$. Equation (16) gives an approximation of the GB Gibbs free energy based on which we are able now to construct the GB phase diagram.

To demonstrate the application of the current density-based model, Pt-Au system is qualitatively studied which largely behaves like a regular solid solution. In the following, a GB with $\rho^{GB} = 0.75$ is considered. In Pt-Au system, the only difference to the theoretical regular solution is in the enthalpy of mixing that extends to the second term in Redlich-Kister polynomial. This makes the mixing coefficient Ω to be composition-dependent as

$$\Omega_{PtAu} = L_0 + L_1(X_{Pt}^B - X_{Au}^B) \quad (17)$$

that enters the formalism above without affecting the model:

$$G_{SS}^{GB} = X_{Pt}^{GB} (H_{Pt}^B (\rho^{GB})^2 - TS_{Pt}^B (\rho^{GB})) + X_{Au}^{GB} (H_{Au}^B (\rho^{GB})^2 - TS_{Au}^B (\rho^{GB})) + (\rho^{GB})^2 \Omega_{PtAu} X_{Pt}^{GB} X_{Au}^{GB} - T \Delta S_{mix}^B \quad (18)$$

Grolier *et al.* [60] have assessed the bulk thermodynamic data for binary Pt-Au and reported $L_0 = 11625 + 8.3104 T$, $L_1 = -12616 + 5.8186 T$ [J/mol] for FCC Pt-Au solid solution. The rest of the thermodynamic data for pure Pt and Au are extracted from SGTE compilation by Dinsdale [61]. Inserting these values in Eqs. (17) and (18) one obtains the Gibbs free energy as a function of GB density and composition. Figure 2 shows a 3D map of the Gibbs free energy for Pt-Au system at 300 K as a function of composition and GB density. It is found that as the GB density decreases, the GB Gibbs free energy increases and deviates larger from the corresponding bulk values. Fig. 3 compares bulk and GB Gibbs free energy for $\rho^{GB} = 0.75$ at different temperatures.

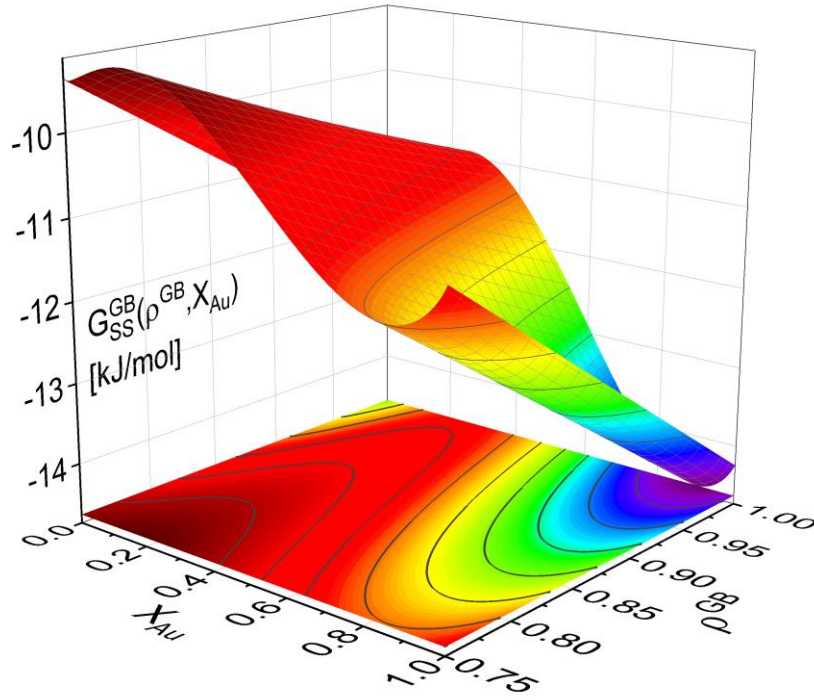


Figure 2: Gibbs free energy of Pt-Au system obtained based on the current density-based model (Eq. (18)) as a generalized function of composition and GB density is shown at $T = 300$ K. For $\rho^{GB} = 1 = \rho^B$, the Gibbs free energy of the bulk is recovered. For $\rho^{GB} < 1$ the free energy values increase.

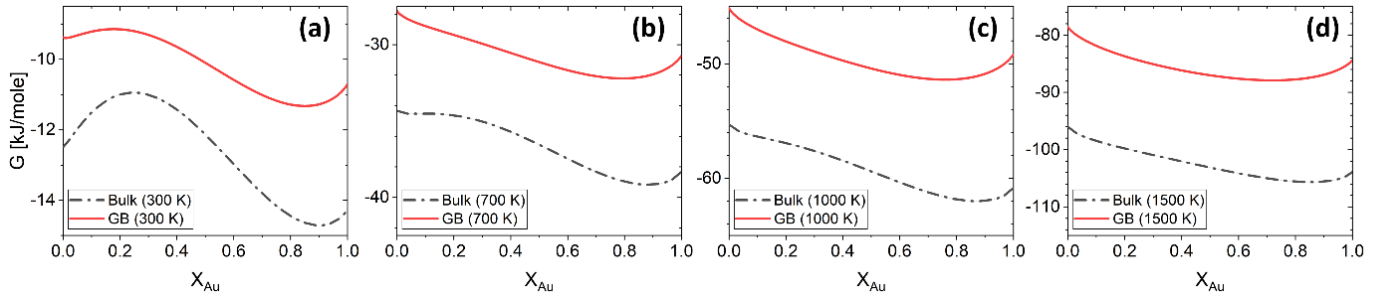


Figure 3: The Gibbs free energy of the bulk and a GB ($\rho^{GB} = 0.75$) in Pt-Au system obtained from Eq. (18) are shown for different temperatures. As expected, the GB Gibbs free energy is higher than the bulk.

Using Eq. (18), the equilibrium phase diagrams of the bulk and any specific GB (with a given density) in Pt-Au system can be generated. Figure 4 compares the equilibrium bulk and GB (with $\rho^{GB} = 0.75$) phase diagrams. Here only the relevant part of the phase diagram, i.e. the FCC Pt-Au solid solution, is plotted. The results show that, inside a GB, the phase separation becomes possible but for limited ranges of temperature and composition when compared to the bulk phase diagram.

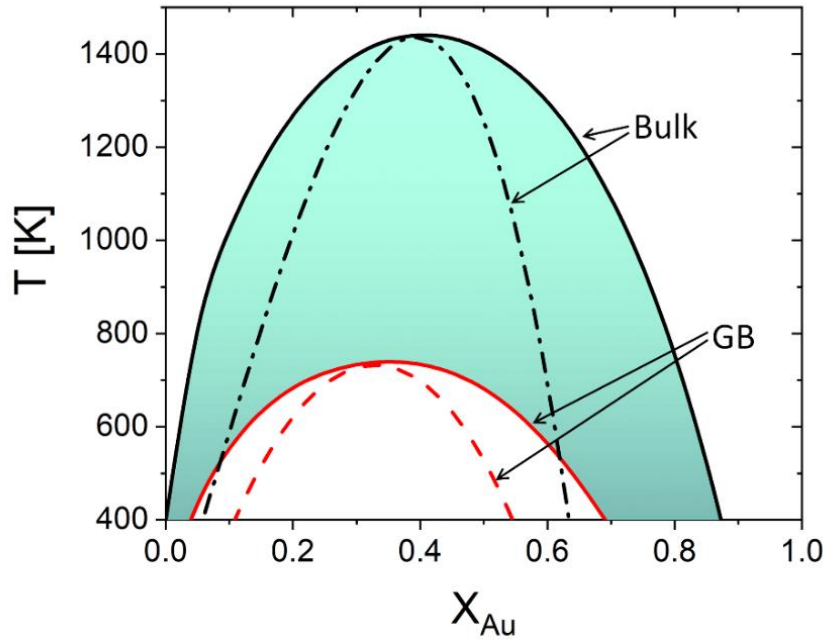


Figure 4: Equilibrium phase diagram for the bulk $\rho = \rho^B = 1$ and an example GB with $\rho = \rho^{GB} = 0.75$ are obtained for Pt-Au system. The dash lines represent the chemical spinodals. The colored region marks the possible domain where the phase diagram for GBs with $0.75 < \rho^{GB} < 1$ can appear. Note that the equilibrium bulk and GB phase diagrams in this figure are plotted independently. The coexistence of the bulk and GB phases will be discussed in Secs. 3.2 and 4.1 and Fig. 6.

As it is evident from the Gibbs free energy plots (Figs. 2 and 3), the GB thermodynamics strongly depend on the GB density ρ^{GB} which represents the nature (type) of the GB (see Sec. 4.2). Although the phase diagram is a nonlinear function of the GB density, the possible values for GB density ρ^{GB} are finite and confined to the area between a minimum GB density and bulk phase diagrams (colored area in Fig. 4). Thus, once the range of GB density is determined, the equilibrium GB phase diagrams can be approximated. Also, it is worth noting that using Eq. (7), the GB density and energy are interchangeable parameters. These aspects of the model are discussed in Sec. 4.2.

3.2 GB segregation behavior

Since GBs only exist together with a bulk phase, their equilibrium phase diagram as presented in Sec. 3.1. will not be useful, unless the coexistence between the GB and bulk phases is understood as well. In a binary system, the coexistence of the GB and bulk phases requires equality of the chemical potentials $\mu_B^B - \mu_A^B = \mu_B^{GB} - \mu_A^{GB}$ all across the system [30]. In reality, these are not the sufficient conditions as a minimum energy state with respect to the density must be satisfied as well. Similar to the previous section, however, if we consider the material point at the center of a flat GB where $\rho = \rho^{GB}$, $\nabla\rho(x=0) = 0$ and $\nabla X_B(x=0) = 0$, we can simplify the problem and solve for the equality of the (relative) chemical potentials using Eq. (16) which gives

$$\begin{aligned} & \frac{X_B^{GB}}{1 - X_B^{GB}} \\ &= \frac{X_B^B}{1 - X_B^B} \cdot \exp \left(- \frac{[\Delta H^B + \Omega](\rho^{GB^2} - 1) - T\Delta S^B(\rho^{GB} - 1) + 2\Omega[X_B^B - \rho^{GB^2}X_B^{GB}]}{RT} \right) \end{aligned} \quad (19)$$

where X_B^{GB} is the composition of the GB at its center with $\rho = \rho^{GB}$, X_B^B is the composition of the bulk far from the GB, $\Delta S = S_B^B - S_A^B$ and $\Delta H^B = H_B^B - H_A^B$. Equation (19) resembles the well-known Fowler-Guggenheim segregation isotherm [30] but also takes the specific effect of a given GB, represented by its density, into account. One can realize that Eq. (19) only uses the bulk thermodynamic data to study GB segregation. For the Pt-Au system we obtain

$$\begin{aligned}
& \frac{X_{Au}^{GB}}{1 - X_{Au}^{GB}} \\
&= \frac{X_{Au}^B}{1 - X_{Au}^B} \\
& \cdot \exp \left(- \frac{[\Delta H^B + L_0] (\rho^{GB^2} - 1) - T \Delta S^B (\rho^{GB} - 1) + 2L_0 [X_{Au}^B - \rho^{GB^2} X_{Au}^{GB}] + Q}{RT} \right)
\end{aligned} \tag{20}$$

with $Q = L_1 [2\rho^{GB^2} X_{Au}^{GB} (1 - X_{Au}^{GB}) - (1 - 2X_{Au}^{GB})^2 - 2X_{Au}^B (1 - X_{Au}^B) + (1 - 2X_{Au}^B)^2]$, $\Delta S = S_{Au}^B - S_{Pt}^B$ and $\Delta H^B = H_{Au}^B - H_{Pt}^B$.

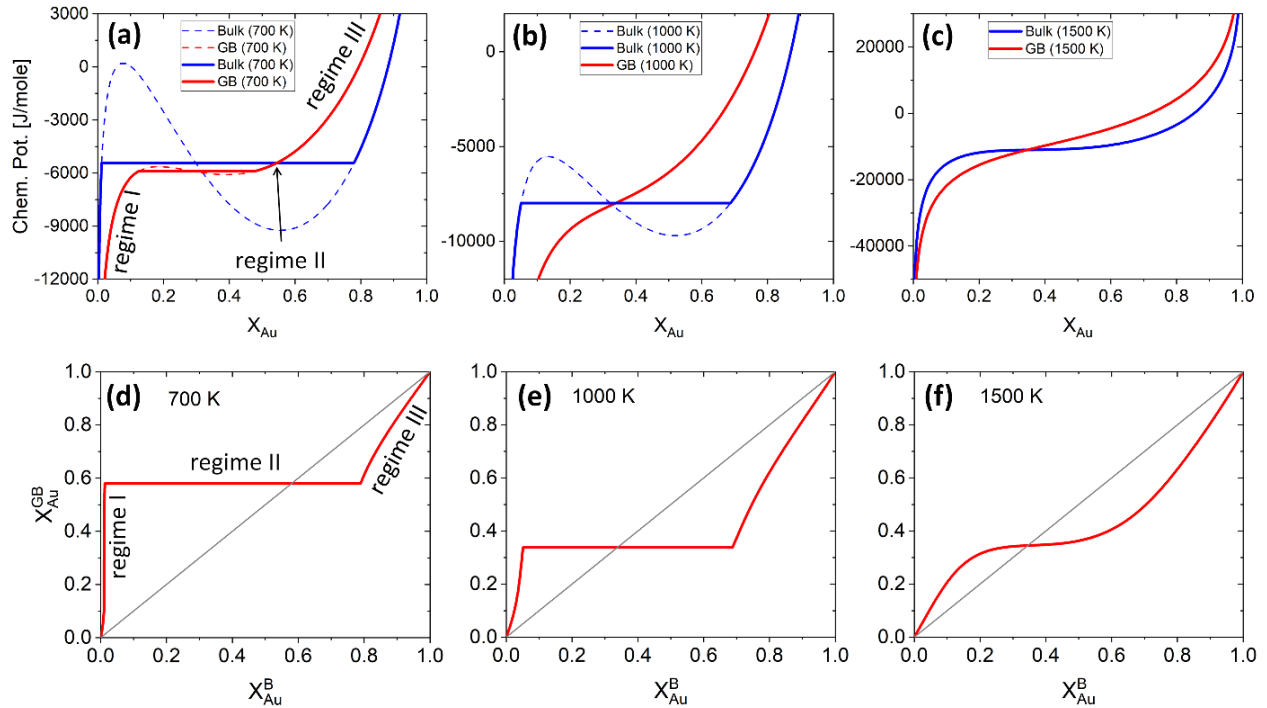


Figure 5: (a)-(c) The chemical potentials of Au atoms in bulk and a GB (with $\rho^{GB} = 0.75$) Pt-Au are plotted for three different temperatures. (d)-(f) Using the parallel tangent condition the segregation isotherms are obtained for the corresponding temperatures. Different regimes of segregation appear depending on the GB density and temperature. See discussions in Sec. 4.2.

For studying the coexistence of the bulk and GB phases, plotting the chemical potential curves and segregation isotherms is very useful. Figure 5 presents the (relative) chemical potentials and the segregation

isotherms for the bulk and an example GB with $\rho^{GB} = 0.75$ in Pt-Au system at three different temperatures. The chemical potential of the GB is a function of GB density and significantly differs from the corresponding bulk chemical potential. The Maxwell construction (defining the two-phase regions) and the spinodal compositions for both GB and bulk materials are shown in Figure 5. It is found that the GB spinodal decomposition can occur for lower values of chemical potential below the bulk spinodal (e.g. in Fig. 5 (a)). As a result, the two-phase GB can be in equilibrium with a single-phase bulk. In Pt-Au system, it has been reported that a segregation-assisted GB phase separation can occur which results in formation of two-phase GBs coexisting with a single-phase bulk [62, 63].

Similarly, the results in Figure 5 show that the two-phase bulk will be in equilibrium with a single-phase GB. In fact, at a given temperature, for any bulk composition within the two-phase region of the phase diagram, the bulk is expected to be in equilibrium with a single phase/composition GB. These are the results of a vertical shift in the GB chemical potential (with respect to the bulk chemical potential) that can be seen in Fig. 5 (a). Combining these results with the equilibrium GB phase diagram (Sec. 3.1), we are able now to study GB thermodynamic phase equilibria as will be further discussed in Sec. 4.1.

4. Discussion

4.1 Coexistence of GB and bulk phases

The current density-based model offers a method to approximate Gibbs free energy of a given GB using the available bulk thermodynamic data. In this model, the GB region is described by a continuous variation of the density field. This continuity allows to simplify the equilibrium GB thermodynamics in the GB center where the gradient term $\nabla\rho$ vanishes (Figure 1 (a) and (b)). Although the results of the current model are then obtained for a single material point within the GB region, the method is applicable for a full-field simulation of the GBs as well, where the temporal variation of density and concentration fields and their gradients can be numerically computed.

In the current study, we focus on the equilibrium GB properties. The current density-based model allows to extend the concept of equilibrium phase diagram for GBs (see Sec. 3.1). Figure 4 presents the equilibrium GB phase diagram for the bulk and a GB (with $\rho^{GB} = 0.75$) in Pt-Au solid solution. The results show that like the bulk materials, GBs can also undergo a spinodal phase separation that is confined to smaller temperature and composition ranges. The difference between the bulk and GB properties depends on the GB density. As the GB density deviates larger from the bulk density, the GB two-phase region in the phase diagram becomes smaller.

The coexistence of bulk and GB phases can be studied using the equal chemical potential condition [30, 64]. In the usual case, the bulk, which is the dominant part of the microstructure, imposes the ultimate thermodynamic states and behavior of the GBs. In Sec. 3.2, the GB-bulk coexistence was discussed using the current density-based model. According to Eq. (19) (or Eq. (20) for the Pt-Au system), the GB segregation level depends on the temperature, bulk composition, as well as GB type represented by its density ρ^{GB} . For a regular solution discussed here, the driving forces for the segregation can be divided into two parts: The first contribution is the ideal segregation energy $\Delta H^B (\rho^{GB^2} - 1) - T\Delta S^B (\rho^{GB} - 1)$ that is analogous to the segregation driving force in Langmuir-McLean isotherm [64]. In fact, if we neglect the energetic contributions due to mixing ($\Omega = 0$), we get a version of Langmuir-McLean relation from Eq. (19):

$$\frac{X_B^{GB}}{1 - X_B^{GB}} = \frac{X_B^B}{1 - X_B^B} \cdot \exp \left(- \frac{\Delta H^B (\rho^{GB^2} - 1) - T\Delta S^B (\rho^{GB} - 1)}{RT} \right) \quad (21)$$

that is now applicable for a given GB with specific density. According to the current model, it was shown that inside the GB region the enthalpy and the entropic part of the segregation energy scale differently with the local density (Eq. (8)). The second contribution in Eq. (19) is due to the mixing $\Omega (\rho^{GB^2} - 1) + 2\Omega [X_B^B - \rho^{GB^2} X_B^{GB}]$ which contains a term with the GB concentration X_B^{GB} . The two contributions discussed above can have cooperative or competitive effects on the segregation level depending on the magnitude and sign of Ω and ΔH^B .

Combining the equilibrium GB phase diagram and the GB segregation isotherms, one can now describe the thermodynamic behavior of GBs. Figure 5 presents the chemical potentials and segregation isotherms for the exemplified Pt-Au system. In this system, three regimes of bulk-GB coexistence could be identified as a function of bulk composition. First, a segregation to the GB occurs as the Au content increases in Pt-rich alloys (regime I). For a two-phase bulk the GB composition becomes fixed (regime II) that applies for the entire range of bulk composition in the two-phase bulk region. Any further increase of the Au content results in solute depletion in the GB (regime III) with respect to the bulk. The segregation isotherm in Fig. 5 (d) shows different regimes of segregation.

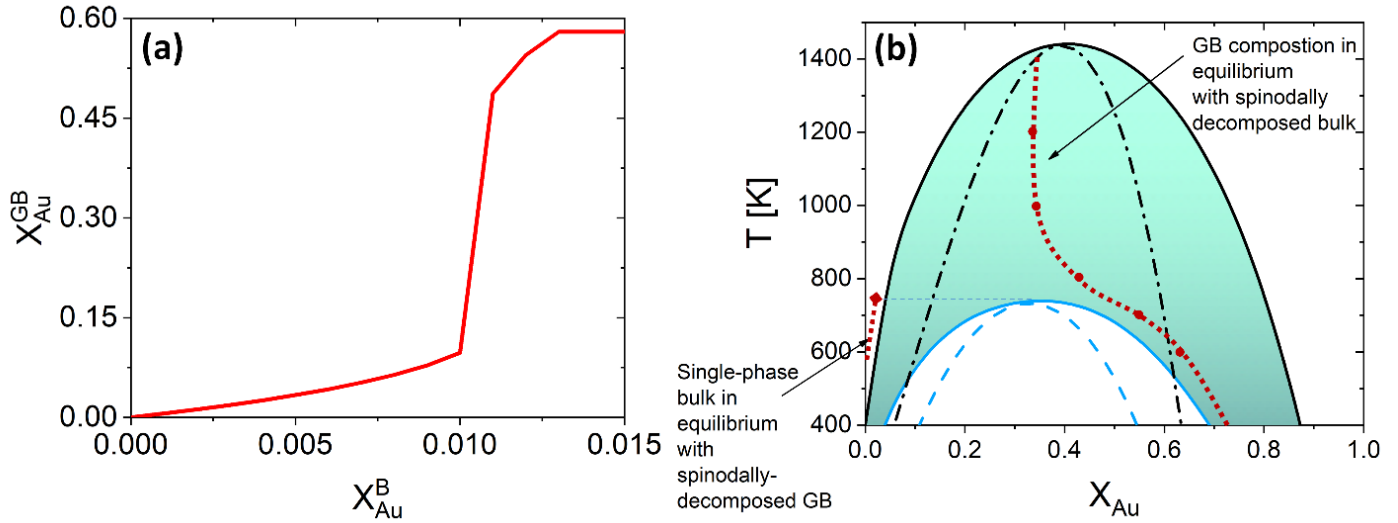


Figure 6: (a) For Pt-Au system at 700 K, a jump (GB spinodal) occurs before the bulk spinodal decomposition takes place. This is a zoomed in plot in Fig. 5 (d) (left corner), see also Fig. 5 (a). (b) Based on the current density-based model the coexistence of the bulk and GB phases is depicted in the phase diagram for the Pt-Au system. A two-phase bulk will be in equilibrium with a single-phase GB while a two-phase (spinodally-decomposed) GB is shown to be in equilibrium with a single-phase bulk.

For a dilute Pt-Au alloy (regime I), it is possible that the GB, which is enriched in Au due to the segregation, undergoes a spinodal decomposition before a bulk decomposition becomes possible. At 700 K, for instance, a GB spinodal transition is indeed revealed in Pt-Au system (see Fig. 4). For a given bulk composition in this temperature, the GB decomposes into low-concentration and high-concentration areas that are in equilibrium with a single-phase bulk. Figure 6 (a) shows a sharp jump in the GB composition as a function of bulk composition (this is a zoomed-in plot of Fig. 5 (d)). The jump in the GB composition indicates that for a specific bulk composition (in the single-phase region of phase diagram) a spinodally-decomposed two-phase GB will form. A segregation-assisted GB spinodal decomposition has been indeed reported recently in nanocrystalline Pt-Au alloy [62]. Atomistic simulations of Pt-Au system confirmed the GB spinodal phase transition for bulk compositions well below the bulk spinodal range [63] which is consistent with the current predictions. Spinodal phase separation is also evidenced in other material systems [65] with technological significance [66, 67]. For the two-phase Pt-Au bulk materials (in regime II), the current model predicts that a single-phase GB will come to coexist. This is because of the vertical shift in the GB chemical potential with respect to the corresponding bulk chemical potential curve, as demonstrated in Fig. 5 (a). Figure 6 (b) summarizes the results of the current study.

The discontinuous jump in the GB segregation isotherm (Fig. 6 (a)) is a result of the difference in the free energy functional and chemical potentials of the bulk and GB phases. In general, the GB chemical potential and its corresponding spinodal decomposition can lie ‘Above’ or ‘Below’ the bulk spinodal, with reference to the chemical potential curves. Figure 7 presents the two cases schematically: If the GB spinodal is ‘Below’ the bulk spinodal then $X_B^{BS1} > X_B^{B*}$ as in the Pt-Au system discussed above. If the GB spinodal lies ‘Above’ the bulk spinodal, a gradual addition of element A (solvent) leads to its segregation and GB spinodal $X_A^{BS2} < X_B^{B*}$. In either case, one can activate a segregation-assisted phase separation in the GB region, that can act as a precursor for subsequent phase transformation, before reaching the bulk spinodal region. In another study, we have shown that a segregation-assisted transient spinodal phase separation can occur at GBs for a larger range of bulk composition [51].

The equilibrium GB phase diagram and segregation behavior depend on the GB density ρ^{GB} . In a polycrystalline material with a large number of GBs of various types (with different crystallographic properties), the local GB density is expected to differ from one GB to another. A quantitative application of the current model, therefore, requires determination of the GB densities of different types. For this purpose, atomistic simulations can provide the necessary means to evaluate GB density profiles. Though atomistic simulations of GBs is beyond the scope of this study, the relationship between the ρ^{GB} and GB free volume and misorientation angle will be briefly discussed in the following.

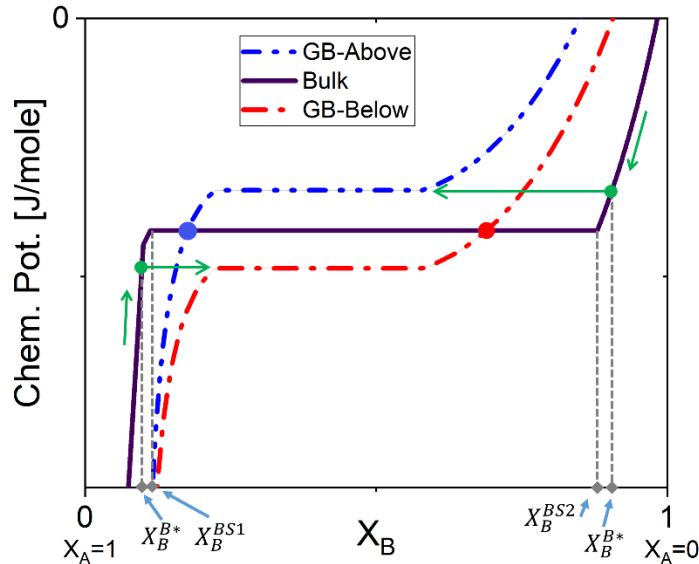


Figure 7: The GB chemical potential can be ‘Below’ or ‘Above’ the bulk’s curve. The two-phase GB will be in equilibrium with a single-phase bulk material as marked by the arrows. The dots on the bulk chemical potential curve indicates the single-phase GB is equilibrium with the two-phase bulk.

4.2 The relation between the GB density and GB nature

In order to make use of the current model, it is helpful to understand the significance of the average GB density ρ^{GB} and its relation with the GB nature. For a flat GB in a pure substance, the GB width 2η depends on the potential energy $-\frac{A}{2}$ and the gradient coefficient κ_A . While the first parameter is a property of the bulk material, the latter maintains the physical length scale of our mesoscale model that depends on the way density is calculated/measured in a system. One way to calculate the density profiles for different GBs is to perform atomistic simulations of GBs. A 3D density map can be extracted from the equilibrium GB configuration using, for instance, a systematic coarse-graining of the atomistic structure. For a short coarse-graining radius, the GB width is expected to become smaller and the density fluctuations (scatters) become larger. On the contrary, a large coarse-graining radius gives smoother density profile and a larger GB width. This allows a tunable modeling of the GB that can be very useful for continuum full-field studies. An application of the current density-based model combined with atomistic simulations, thermodynamic databases and experimental measurements will be published elsewhere [51].

For a flat GB, Eq. (7) relates the GB energy γ to its density ρ^{GB} which is extremely helpful in establishing physical relations between the initial GB energy and other GB thermodynamic properties, especially its tendency for segregation. Using Eqs. (7) and (15), the GB Gibbs free energy of a regular solution can be written as a function of its initial GB energy. Accordingly, we can rewrite Eq. (19) as

$$\frac{X_B^{GB}}{1 - X_B^{GB}} = \frac{X_B^B}{1 - X_B^B} \cdot \exp \left(- \frac{[\Delta H^B + \Omega] \left(\left[1 - \sqrt{\frac{\gamma}{\alpha_0}} \right]^2 - 1 \right) - T \Delta S^B \left(\left[1 - \sqrt{\frac{\gamma}{\alpha_0}} \right] - 1 \right) + 2\Omega \left[X_B^B - \left[1 - \sqrt{\frac{\gamma}{\alpha_0}} \right]^2 X_B^{GB} \right]}{RT} \right) \quad (22)$$

that gives a useful relation for describing the tendency of GB segregation as a function of its initial energy. In fact, this is observed that GBs with higher energies attract more solute content during the segregation [68].

Another way to interpret the GB density parameter is the concept of GB free volume. In order to relate the GB free volume ΔV (per unit area) with the GB density ρ^{GB} , we need to map the ‘excess’ volume to the ‘shortage’ of mass in the GB. Comparing a GB against the bulk of the same volume and using Eq.

(6), for the unit area of a flat GB as depicted in Fig. 1 (a) and (b), the relative mass of the GB will be $m^{GB} = \frac{(1+\rho^{GB})}{2}$ (where $m^B = 1$) and the relative mass difference with respect to the bulk will be

$$\Delta m = 1 - \rho^{GB} \quad (23)$$

where $m = 2 \int_0^\eta \rho(x) dx$ is the total relative mass of the considered domain. Comparing Eq. (23) with the GB free volume per unit area, defined as $\Delta V = \frac{WN^B}{N_0} \left(1 - \frac{N^{GB}}{N^B}\right)$ [69], one can find the one-to-one relationship between Δm and ΔV . Here W is the atom diameter, N^{GB} is the number of atoms in the GB, N^B is the number of atoms in the bulk within the same volume and N_0 is the number of atoms per unit area of the GB. As the fraction $\frac{N^{GB}}{N^B}$ is analogous to ρ^{GB} we obtain $\Delta V \propto (1 - \rho^{GB}) = \Delta m$. Extensive works have been devoted to calculate and measure the GB free volume (see for instance [70-72]). In fact, Aaron and Bolling [69] have shown that the energy of different types of GBs can be associated with their free volume which, in principle, can be extended as well for the GB density parameter proposed here.

Theoretically, the maximum GB density value is the corresponding bulk density $\rho = \rho^B = 1$. Special GBs such as coherent twin boundaries (TBs) with low coincidence values show small GB energy and free volumes [69]. This is well consistent with the current model in which as ΔV goes to zero, ρ^{GB} approaches $\rho^B = 1$ and γ approaches zero (Eq. (7)). For a low-angle GB (LAGB), the situation becomes a bit more complex as the GB energy and density are related to the presence of dislocations. Since dislocations are localized defects with a lower atomic density in their core, one expects the local GB density ρ^{GB} within the LAGB plane to fluctuate accordingly. Although it is not possible to apply the current density model to the local density variation within the GB plane on the atomic scale, we still can approximate the average GB density for a LAGB by a simple volume averaging of regularly spaced dislocations. For a tilt GB, a simple geometrical construction of a LAGB gives the average GB density $\rho_{tilt}^{GB} \approx 1 - \frac{\sin \theta}{4}$ with the GB misorientation θ , and the edge dislocation core density $\rho^D \approx 0.75$ (see Appendix C for detailed derivations), i.e. the density of GB decreases as its misorientation increases. This results in a misorientation-dependent mass difference at the GB as $\Delta m \approx \frac{\sin \theta}{4}$ and thus a corresponding GB free volume $\Delta V \propto \sin \theta$ that is indeed consistent with the previous studies [69, 73].

According to the current density-based model, the GB isotherms and equilibrium phase compositions depend on the GB density (Eqs. (18) and (20)) and therefor GB misorientation. The dependency of GB segregation on the GB misorientation in Pt-Au system has been studied in several previous works. Seki *et*

al. [74, 75] and Seidman [76] studied Au segregation to twist boundaries and have shown that although the GB segregation is not homogeneous, its average level increases as the misorientation angle increases (with the exception of special GBs) which is consistent with the current results. In a recent atomistic study of nanocrystalline Pt-Au, O'Brian *et al* [63] have also shown that different levels of segregation can occur in different types of GBs.

In order to set the lower limit of the GB density value (highest free volume), we need to consider general high angle GBs (HAGBs). The relative density of a smooth free surface can be approximated to be 0.5 (that can of course be lower or higher depending on the way atoms relax on the surface). For a HAGB buried inside the bulk (with exception of special GBs), however, one expects significant interaction among the atoms from the two surfaces brought together at the GB that results in a higher GB density and lower GB energy. In fact, it is proposed that the energy of a HAGB is lower than (about $\frac{1}{3}$ of) the surface energy in the same substance [77] that, according to Eq. (7), necessarily results in a density much higher than 0.5 corresponding to a free surface. Arron and Bolling remarked that the free volume in a HAGB is comparable to that of a liquid phase [69]. In our calculations presented above, we have used $\rho^{GB} = 0.75$ for computing the GB phase diagram and segregation behavior. A comprehensive study of GB density and its relation with the GB nature requires performing atomistic simulations which is left for a future study.

5. Summary and outlook

A density-based model for assessing GB thermodynamics is proposed. The current model uses the available bulk thermodynamic data as input and gives a rather general formulation for the GB Gibbs free energy. Using this formulation, the phase diagram of GBs in contact with their corresponding bulk phase(s) were obtained. The model was qualitatively demonstrated for Pt-Au system. The results show that in a Pt-rich alloy (i) Au atoms segregate to the GB where (ii) the average level of segregation increases with the misorientation angle (with the exception of special GBs) and (iii) a GB spinodal decomposition can occur for a bulk composition below the bulk spinodal point. A comparison to the previous studies on Pt-Au system confirms these conclusions. The relationships between GB density, GB free volume and GB misorientation were also discussed. The current density-based model offers a powerful tool to develop GB thermodynamic databases based on the existing bulk thermodynamic data. This requires systematic studies of density profiles for different types of GBs as well as their coexistence. Furthermore, GB elastic energy contribution and segregation in multicomponent alloys are left to be discussed in a future study. An application of this

model enables knowledge-based studying and design of polycrystalline materials by segregation engineering of GBs.

Appendix A: Density-based Gibbs Free Energy Functional

The Gibbs free energy functional of a monatomic system made of atoms A, over the domain Ω can be written as

$$\Phi = \int_{\Omega} \rho_m g_A(\rho) dV = \int_{\Omega} \rho_m (E + K + pV - TS) dV \quad \text{A.1}$$

where ρ_m is mass density, E is potential energy, K is kinetic energy, p is pressure, V is volume, T is temperature and S is entropy. Here Φ has the dimension of energy, Joule, $g_A(\rho)$ and energetic terms inside the parenthesis are per unit mass and the entire term under the integral is Joule per unit volume. The objective of this appendix is to find the Gibbs free energy functional of a monatomic system with some density variation (having a GB in the system) and under the assumption of a continuous density profile. While the kinetic energy, the mechanical work and the entropic term locally scale with the mass density in Eq. A.1, the potential energy E needs a further analysis as it is a function of the nonlocal atomic interactions.

Let us begin with a simple system, i.e. a planar GB (a 1D symmetry breaking surface) separating two infinitely large and homogeneous grains. In general, the potential energy density in any given point x within the system can be defined as

$$E(x) = E(-\infty) + \frac{1}{2} \int_{-\infty}^x f(r) dr \quad \text{A.2}$$

where $E(-\infty)$ is the potential energy inside the homogeneous grain (at $r = -\infty$) and the integral describes the work done on the matter to bring it from $r = -\infty$ to a given position $r = x$, half of which then will be stored in the material point. $f(r)$ is the total force density applied on any point r that is the integral of all possible interactions between atoms:

$$f(r) = \int_0^{\infty} [\zeta(r+q) - \zeta(r-q)] dq \quad \text{A.3}$$

Here $\zeta(r \pm q)$ is the force density at point r due to interaction with another material point separated by $\pm q$ in space. All forces are attractive as displayed in the sign of the $\zeta(r \pm q)$ terms. One can then assume the force density to have a functional form

$$\zeta(r \pm q) = \frac{\alpha m(r \pm q)}{q^n} = \psi(q) \rho_m(r \pm q) \quad \text{A.4}$$

where α is a material constant, m is mass and $\psi(q) = \frac{\alpha V_L}{q^n}$. In this formulation, V_L is the volume over which the density field is defined, that is equivalent to the characteristic coarse-graining volume. Equation A.4 is inspired by the general force relations (such as Coulomb relation, also resembled in interatomic potentials) with $n > 1$. Inserting Eq. A.4 in Eq. A.3 and integrating by part give

$$\begin{aligned} f(r) &= \int_0^\infty \psi(q) [\rho_m(r+q) - \rho_m(r-q)] dq \\ &= \psi(q) [\rho_m(r+q) - \rho_m(r-q)]_0^\infty - \int_0^\infty \psi(q) \frac{\partial [\rho_m(r+q) - \rho_m(r-q)]}{\partial q} dq \\ &= - \int_0^\infty \psi(q) \frac{\partial [\rho_m(r+q) - \rho_m(r-q)]}{\partial q} dq \end{aligned} \quad \text{A.5}$$

where $\lim_{q \rightarrow \infty} \psi(q) = 0$ and $\lim_{q \rightarrow 0} [\rho_m(r+q) - \rho_m(r-q)] = 0$ were used. Applying the Tylor expansions $\rho_m(r \pm q) = \rho_m(r) \pm \frac{\partial \rho_m}{\partial r} q + \frac{1}{2!} \frac{\partial^2 \rho_m}{\partial r^2} q^2 \pm \frac{1}{3!} \frac{\partial^3 \rho_m}{\partial r^3} q^3 + \dots$ the partial derivatives of density fields in Eq. A.5 will be

$$\frac{\partial \rho_m(r \pm q)}{\partial q} = \pm \frac{\partial \rho_m}{\partial r} + \frac{\partial^2 \rho_m}{\partial r^2} q \pm \frac{1}{2!} \frac{\partial^3 \rho_m}{\partial r^3} q^2 + \dots \quad \text{A.6}$$

Inserting then Eq. A.6 into Eq. A.5 gives

$$\begin{aligned} f(r) &= - \int_0^\infty \psi(q) \left[2 \frac{\partial \rho_m}{\partial r} + \frac{\partial^3 \rho_m}{\partial r^3} q^2 + \dots \right] dq \\ f(r) &= -A \left[\frac{\partial \rho_m}{\partial r} \right] - \kappa \left[\frac{\partial^3 \rho_m}{\partial r^3} \right] - \dots \end{aligned} \quad \text{A.7}$$

with $A = \int_0^\infty 2 \psi(q) dq$ and $\kappa = \int_0^\infty \psi(q) q^2 dq$ that are model parameters. Thus

$$\begin{aligned} \frac{1}{2} \int_{-\infty}^x f(r) dr &= \frac{1}{2} \int_{-\infty}^x \left[-A \left[\frac{\partial \rho_m}{\partial r} \right] - \kappa \left[\frac{\partial^3 \rho_m}{\partial r^3} \right] - \dots \right] dr \\ &= -\frac{A}{2} \rho_m \Big|_{-\infty}^x - \frac{\kappa}{2} \frac{\partial^2 \rho_m}{\partial r^2} \Big|_{-\infty}^x - \dots = -\frac{A}{2} (\rho_m(x) - \rho_m(-\infty)) - \frac{\kappa}{2} \left(\frac{\partial^2 \rho_m}{\partial r^2} \right)_x - \dots \end{aligned} \quad \text{A.8}$$

with $\left(\frac{\partial^2 \rho_m}{\partial r^2} \right)_{-\infty} = 0$ and from Eq. A.2 we get

$$E(x) = -\frac{A}{2} \rho_m(x) - \frac{\kappa}{2} \left(\frac{\partial^2 \rho_m}{\partial r^2} \right)_x - \dots \quad \text{A.9}$$

with $E(-\infty) = -\frac{A}{2} \rho_m(-\infty)$. As a consequence of this treatment, it is clear that the fourth and higher (even) order derivatives of the density field can still contribute to the potential energy. These are however omitted in the following. Inserting Eq. A.9 in Eq. A.1 we obtain

$$\Phi = \int_{\Omega} \left[-\frac{A}{2} \rho_m^2 + \frac{\kappa}{2} (\nabla \rho_m)^2 + \rho_m (K + pV - TS) \right] dV \quad \text{A.10}$$

where we used a three dimensional notation for ρ_m and $\nabla \rho_m$ and, $\int (\nabla \rho_m)^2 dV = -\int \rho_m \nabla^2 \rho_m dV$ with $\nabla \rho = 0$ at the boundaries of the integral. Equation A.10 gives the description of a monatomic single phase with a spatial density variation. Without losing any generality, we perform now two simplifying rescaling: (i) we rescale the density parameter with its corresponding value in the bulk grain $\rho_m^B = \rho_m(-\infty)$ to obtain a relative density parameter ρ and (ii) switch to the more applied energy unit per unit mole, G_A , where we have $\frac{G_A}{V_m} = \rho_m g_A(\rho) = -\frac{A}{2} \rho^2 + \frac{\kappa}{2} (\nabla \rho)^2 + \rho (K + pV - TS)$. Hence

$$G_A = -\frac{A_A}{2} \rho^2 + \frac{\kappa_A}{2} (\nabla \rho_A)^2 + \rho (K_A + pV_A - TS_A) \quad \text{A.11}$$

where

$$\rho(x) = \frac{\rho_m(x)}{\rho_m^B},$$

A.12

$$A_A = AV_m\rho_m^B, \kappa_A = \kappa V_m\rho_m^B, K_A = KV_m\rho_m^B, S_A = SV_m\rho_m^B$$

For the rest of derivations and discussions about the current model please see Sec. 2.1.

Appendix B: Equilibrium GB Density Profile

The equilibrium GB profile across a GB in a pure substance can be obtained by minimizing the free energy functional (Eq. (1)) using Eq. (5) with respect to the relative density. For a 1D setup,

$$\frac{\delta\Phi}{\delta\rho} = \frac{\partial\Phi}{\partial\rho} - \frac{\partial}{\partial x} \left(\frac{\partial\Phi}{\partial(\partial\rho/\partial x)} \right) = -A\rho + B - \kappa_\rho \frac{\partial^2\rho}{\partial x^2} = 0 \quad \text{B.1}$$

where $B = K_A + pV - TS_A$ (see Appendix A as well). The general solution for this second-order linear ordinary differential equation reads

$$\rho(x) = \frac{B}{A} + C_1 \cos\left(\sqrt{\frac{A}{\kappa_\rho}} x\right) + C_2 \sin\left(\sqrt{\frac{A}{\kappa_\rho}} x\right) \quad \text{B.2}$$

where C_1 and C_2 are constants and

$$\frac{\partial\rho}{\partial x} = \sqrt{\frac{A}{\kappa_\rho}} \left[-C_1 \sin\left(\sqrt{\frac{A}{\kappa_\rho}} x\right) + C_2 \cos\left(\sqrt{\frac{A}{\kappa_\rho}} x\right) \right] \quad \text{B.3}$$

Applying the boundary conditions $\rho(x=0) = \rho^{GB}$, $\rho(x=\pm\eta) = 1$ and the continuity condition $\frac{\partial\rho}{\partial x}(x=0) = 0$ we can relate the three parameters in the model (A , B and κ_ρ) as

$$C_1 = -\frac{1 - \rho^{GB}}{2} \quad \text{B.4}$$

$$C_2 = 0 \quad \text{B.5}$$

$$\eta = \pi \sqrt{\frac{\kappa_A}{A}} \quad \text{B.6}$$

$$\frac{B}{A} = \frac{1 + \rho^{GB}}{2} \quad \text{B.7}$$

The current derivations allow to neglect gradient energy term in the center of GB, $\nabla \rho(x=0) = 0$. In contrast to the current model, common phase-field models for GBs with $\Phi = \int [a_1(1-\phi)^2 + a_2(\nabla \phi)^2] dV$ (or other classical phase-field model with $\Phi = \int [a_1\phi^n(1-\phi)^n + a_2(\nabla \phi)^2] dV$ ($n \geq 1$)) which only have two free parameters, cannot satisfy the boundary conditions $\phi(x=0) = \text{Const}$, $\phi(x = \pm\eta) = \text{Const}$. as well as the continuity condition $\frac{\partial \phi}{\partial x}(x=0) = 0$ at the same time. Please also see Figure 1 and the discussions in Sec. 2.1.

Appendix C: A Simple Geometrical Calculation of LAGB Density

The objective of this appendix is to provide a simple analysis about the LAGB density and its dependence on the misorientation angle. In its simplest form, a LAGB can be mapped with a set of regularly spaced dislocations separated by a distance [57]

$$D = \frac{b}{\sin \theta} \quad \text{C.1}$$

in which b is the Burgers vector of the dislocations and θ is the GB misorientation angle. The ‘average’ relative GB density can be obtained by averaging the density of a dislocation in the unit area of the LAGB. For a tilt LAGB one obtains

$$\rho_{tilt}^{GB} = \frac{Db - bb}{Db} + \frac{bb}{Db} \rho^D \quad \text{C.2}$$

where ρ^D is the relative density at the core of an edge dislocation. Inserting Eq. C.1 in Eq. C.2

$$\rho_{tilt}^{GB} = 1 - (1 - \rho^D) \sin \theta \quad \text{C.3}$$

Here it is assumed that the volume between the two dislocations has the same density as bulk ($\rho^B = 1$), i.e. the elastic effects of the dislocations are neglected. For an edge dislocation depicted in Fig. 8 (a), one can approximate $\rho^D \approx \frac{3}{4} \left(1 + \frac{b}{4a-b}\right)$ where a is the interatomic distance normal to the edge dislocation line. Neglecting the second term inside the parenthesis then we have $\rho^D \approx 0.75$ that gives the density of a tilt GB as

$$\rho_{tilt}^{GB} \approx 1 - \frac{\sin \theta}{4} \quad \text{C.4}$$

In this relation, as θ approaches zero, ρ^{GB} approaches $\rho^B = 1$ and the GB energy (according to Eq. (7)) decreases towards zero. Inserting Eq. C.4 into Eq. (7), we obtain

$$\gamma_{tilt} = \alpha_0 \frac{(\sin \theta)^2}{16} \quad \text{C.5}$$

that is the tilt GB energy as a function of misorientation angle. Equations (7), C.4 and C.5 give the one-to-one relationship between the GB density, energy and misorientation angle based on the current simple analysis. From Eqs. (23) and C.4 the mass difference at the GB is $\Delta m_{tilt} \approx \frac{\sin \theta}{4}$ and thus the corresponding average GB free volume will be proportional to the misorientation angle as $\Delta V \propto \sin \theta$. Figure 8 (b) and (c) show variation of GB density and energy as a function of misorientation angle up to $\theta = 25^\circ$ (with the exception of special GBs).

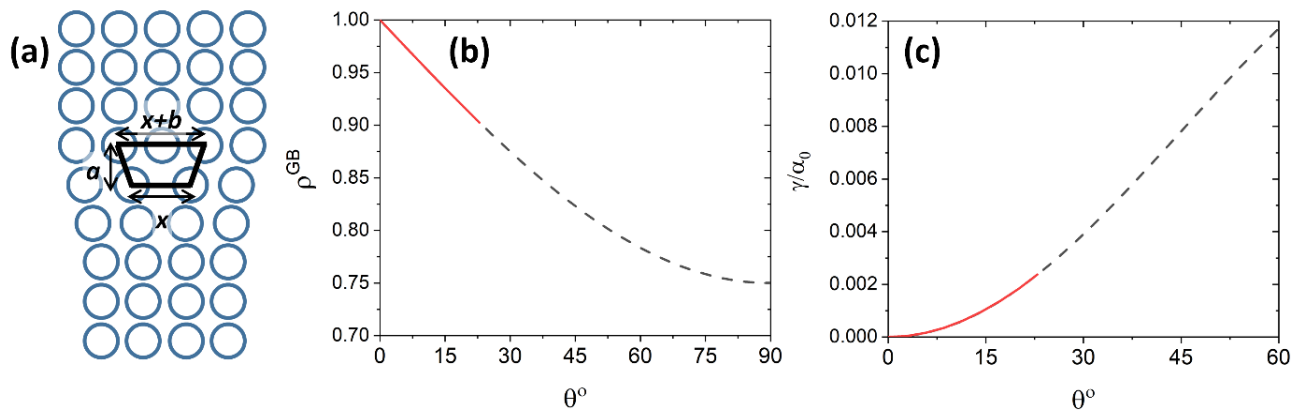


Figure 8: (a) The core of an edge dislocation has a lower density than that of the bulk that is captured by a simple geometrical analysis. GB density (b) and energy (c) as a function of misorientation angle are plotted for a tilt LAGB (Eqs. C.4 and C.5) with the exception of special GBs.

It should be emphasized that Eqs. C.4 and C.5 are based on a very simplified averaging LAGB density and does not account for the elastic energy of the dislocations which can introduce an error specially for obtaining GB energy. Nevertheless, it is useful to show that the current model converges to the expected GB energies in the limiting cases, consistent with the previous derivations of GB energy based on the free volume concept (see [69]). In order to connect the GB segregation isotherm with its initial misorientation angle, we need to replace the density parameter using C.4. From Eqs. C.4 and (16)

$$G_{SS}^{GB} = X_A^{GB} \left(H_A^B \left(1 - \frac{\sin \theta}{4} \right)^2 - TS_A^B \left(1 - \frac{\sin \theta}{4} \right) \right) + X_B^{GB} \left(H_B^B \left(1 - \frac{\sin \theta}{4} \right)^2 - TS_B^B \left(1 - \frac{\sin \theta}{4} \right) \right) \\ + \left(1 - \frac{\sin \theta}{4} \right)^2 \Omega X_A^{GB} X_B^{GB} - T \Delta S_{mix}^B \quad C.6$$

Thus, using Eqs. C.6 and (19) the GB segregation isotherm follows

$$\frac{X_B^{GB}}{1 - X_B^{GB}} \\ = \frac{X_B^B}{1 - X_B^B} \cdot \exp \left(- \frac{[\Delta H^B + \Omega] \left(\left(1 - \frac{\sin \theta}{4} \right)^2 - 1 \right) - T \Delta S^B \left(\left(1 - \frac{\sin \theta}{4} \right) - 1 \right) + 2\Omega \left[X_B^B - \left(1 - \frac{\sin \theta}{4} \right)^2 X_B^{GB} \right]}{RT} \right) \quad C.7$$

Acknowledgement

This work was performed under the project DA 1655/2-1 within the Heisenberg program from the Deutsche Forschungsgemeinschaft (DFG). The author gratefully acknowledges financial supports within this program.

Data Availability

The numerical data from this study are available upon reasonable request.

References

- [1] N. Hansen, Hall–Petch relation and boundary strengthening, *Scripta Materialia* 51(8) (2004) 801-806.
- [2] B. Liu, D. Raabe, P. Eisenlohr, F. Roters, A. Arsenlis, G. Hommes, Dislocation interactions and low-angle grain boundary strengthening, *Acta Materialia* 59(19) (2011) 7125-7134.
- [3] R. Stevens, Grain-boundary sliding in metals, *Metallurgical Reviews* 11(1) (1966) 129-142.
- [4] G. Palumbo, P. King, K. Aust, U. Erb, P. Lichtenberger, Grain boundary design and control for intergranular stress-corrosion resistance, *Scripta Metallurgica et Materialia* 25(8) (1991) 1775-1780.
- [5] R.D. Kamachali, J. Hua, I. Steinbach, A. Hartmaier, Multiscale simulations on the grain growth process in nanostructured materials: Paper presented at the 2nd Sino-German Symposium on Computational Thermodynamics and Kinetics and their Applications to Solidification, *International Journal of Materials Research* 101(11) (2010) 1332-1338.
- [6] R.D. Kamachali, Grain boundary motion in polycrystalline materials, Univ.-Bibliothek, 2013.
- [7] C. Schwarze, R.D. Kamachali, I. Steinbach, Phase-field study of zener drag and pinning of cylindrical particles in polycrystalline materials, *Acta Materialia* 106 (2016) 59-65.
- [8] J. Luo, V. Gupta, D. Yoon, H. Meyer III, Segregation-induced grain boundary premelting in nickel-doped tungsten, *Applied Physics Letters* 87(23) (2005) 231902.
- [9] K.E. Sickafus, S. Sass, Grain boundary structural transformations induced by solute segregation, *Acta Metallurgica* 35(1) (1987) 69-79.
- [10] Y. Yan, M. Chisholm, G. Duscher, A. Maiti, S. Pennycook, S. Pantelides, Impurity-induced structural transformation of a MgO grain boundary, *Physical review letters* 81(17) (1998) 3675.
- [11] D. Vaughan, Grain boundary precipitation in an Al-Cu alloy, *Acta Metallurgica* 16(4) (1968) 563-577.
- [12] M. De Hass, J.T.M. De Hosson, Grain boundary segregation and precipitation in aluminium alloys, *Scripta materialia* 44(2) (2001) 281-286.
- [13] M. Guttman, P. Krahe, F. Abel, G. Amsel, M. Bruneaux, C. Cohen, Temper embrittlement and intergranular segregation of antimony: A quantitative analysis performed with the backscattering of energetic ions, *Metallurgical Transactions* 5(1) (1974) 167.
- [14] R. Messmer, C. Briant, The role of chemical bonding in grain boundary embrittlement, *Acta Metallurgica* 30(2) (1982) 457-467.

- [15] P. Lejček, M. Šob, V. Paidar, Interfacial segregation and grain boundary embrittlement: An overview and critical assessment of experimental data and calculated results, *Progress in Materials Science* 87 (2017) 83-139.
- [16] J.R. Trelewicz, C.A. Schuh, Grain boundary segregation and thermodynamically stable binary nanocrystalline alloys, *Physical Review B* 79(9) (2009) 094112.
- [17] T. Chookajorn, H.A. Murdoch, C.A. Schuh, Design of stable nanocrystalline alloys, *Science* 337(6097) (2012) 951-954.
- [18] S. Hu, L. Chen, Solute segregation and coherent nucleation and growth near a dislocation—a phase-field model integrating defect and phase microstructures, *Acta materialia* 49(3) (2001) 463-472.
- [19] S. Hu, L. Chen, Diffuse-interface modeling of composition evolution in the presence of structural defects, *Computational Materials Science* 23(1-4) (2002) 270-282.
- [20] P.-R. Cha, S.G. Kim, D.-H. Yeon, J.-K. Yoon, A phase field model for the solute drag on moving grain boundaries, *Acta materialia* 50(15) (2002) 3817-3829.
- [21] S. Hu, Y. Li, Y. Zheng, L. Chen, Effect of solutes on dislocation motion—a phase-field simulation, *International Journal of Plasticity* 20(3) (2004) 403-425.
- [22] N. Ma, C. Shen, S. Dregia, Y. Wang, Segregation and wetting transition at dislocations, *Metallurgical and Materials Transactions A* 37(6) (2006) 1773-1783.
- [23] K. Grönhagen, J. Ågren, Grain-boundary segregation and dynamic solute drag theory—A phase-field approach, *Acta Materialia* 55(3) (2007) 955-960.
- [24] S.G. Kim, Y.B. Park, Grain boundary segregation, solute drag and abnormal grain growth, *Acta Materialia* 56(15) (2008) 3739-3753.
- [25] G. Gottstein, L.S. Shvindlerman, Grain boundary migration in metals: thermodynamics, kinetics, applications, CRC press 2009.
- [26] P. Lejček, Grain boundaries: description, structure and thermodynamics, Springer 2010.
- [27] J.W. Gibbs, The Collected Works of J. Willard Gibbs, Ph. D., LLD [Vol 1-2], London, England, Yale University Press 1957.
- [28] I. Langmuir, The adsorption of gases on plane surfaces of glass, mica and platinum, *Journal of the American Chemical society* 40(9) (1918) 1361-1403.
- [29] D. MacLean, Grain boundaries in metals, (1957).
- [30] R.H. Fowler, E.A. Guggenheim, Statistical thermodynamics: a version of statistical mechanics for students of physics and chemistry, The University Press 1939.

- [31] E.W. Hart, Two-dimensional phase transformation in grain boundaries, *Scripta Metallurgica* 2(3) (1968) 179-182.
- [32] E.W. Hart, Grain boundary phase transformations, *The nature and behavior of grain boundaries*, Springer 1972, pp. 155-170.
- [33] M. Guttman, Grain boundary segregation, two dimensional compound formation, and precipitation, *Metallurgical Transactions A* 8(9) (1977) 1383-1401.
- [34] J.W. Cahn, Critical point wetting, *The Journal of Chemical Physics* 66(8) (1977) 3667-3672.
- [35] N. Ma, S. Dregia, Y. Wang, Solute segregation transition and drag force on grain boundaries, *Acta materialia* 51(13) (2003) 3687-3700.
- [36] R. Kobayashi, J.A. Warren, W.C. Carter, A continuum model of grain boundaries, *Physica D: Nonlinear Phenomena* 140(1-2) (2000) 141-150.
- [37] M. Tang, W.C. Carter, R.M. Cannon, Diffuse interface model for structural transitions of grain boundaries, *Physical Review B* 73(2) (2006) 024102.
- [38] M. Tang, W.C. Carter, R.M. Cannon, Grain boundary order-disorder transitions, *Journal of materials science* 41(23) (2006) 7691-7695.
- [39] M. Tang, W.C. Carter, R.M. Cannon, Grain boundary transitions in binary alloys, *Physical review letters* 97(7) (2006) 075502.
- [40] S.G. Kim, J.S. Lee, B.-J. Lee, Thermodynamic properties of phase-field models for grain boundary segregation, *Acta Materialia* 112 (2016) 150-161.
- [41] S.G. Kim, W.T. Kim, T. Suzuki, Phase-field model for binary alloys, *Physical review e* 60(6) (1999) 7186.
- [42] S.J. Dillon, M.P. Harmer, J. Luo, Grain boundary complexions in ceramics and metals: an overview, *Jom* 61(12) (2009) 38-44.
- [43] W.D. Kaplan, D. Chatain, P. Wynblatt, W.C. Carter, A review of wetting versus adsorption, complexions, and related phenomena: the rosetta stone of wetting, *Journal of Materials Science* 48(17) (2013) 5681-5717.
- [44] P.R. Cantwell, M. Tang, S.J. Dillon, J. Luo, G.S. Rohrer, M.P. Harmer, Grain boundary complexions, *Acta Materialia* 62 (2014) 1-48.
- [45] A.P. Sutton, R.W. Balluffi, *Interfaces in Crystalline Materials*, 1995.
- [46] P.E.J. Flewitt, R.K. Wild, Grain boundaries: their microstructure and chemistry, *Grain Boundaries: Their Microstructure and Chemistry*, by PEJ Flewitt, RK Wild, pp. 338. ISBN 0-471-97951-1. Wiley-VCH, April 2001. (2001) 338.

- [47] M.K. Miller, Atom probe tomography: analysis at the atomic level, Springer Science & Business Media 2012.
- [48] M. Herbig, D. Raabe, Y. Li, P. Choi, S. Zaefferer, S. Goto, Atomic-scale quantification of grain boundary segregation in nanocrystalline material, *Physical review letters* 112(12) (2014) 126103.
- [49] L. Huber, R. Hadian, B. Grabowski, J. Neugebauer, A machine learning approach to model solute grain boundary segregation, *npj Computational Materials* 4(1) (2018) 64.
- [50] T.A. Sharp, S.L. Thomas, E.D. Cubuk, S.S. Schoenholz, D.J. Srolovitz, A.J. Liu, Machine learning determination of atomic dynamics at grain boundaries, *arXiv preprint arXiv:1803.01416* (2018).
- [51] R.D. Kamachali, A.K. da Silva, E. McEniry, D. Ponge, B. Gault, J. Neugebauer, D. Raabe, Segregation--Assisted Spinodal and Transient-Spinodal at Grain Boundaries (<https://arxiv.org/abs/1905.07970>), (2019 (Submitted)).
- [52] J.D. van der Waals, The thermodynamic theory of capillarity under the hypothesis of a continuous variation of density, *Journal of Statistical Physics* 20(2) (1979) 200-244.
- [53] L.-Q. Chen, Phase-field models for microstructure evolution, *Annual review of materials research* 32(1) (2002) 113-140.
- [54] I. Steinbach, Phase-field models in materials science, *Modelling and simulation in materials science and engineering* 17(7) (2009) 073001.
- [55] W.J. Boettinger, J.A. Warren, C. Beckermann, A. Karma, Phase-field simulation of solidification, *Annual review of materials research* 32(1) (2002) 163-194.
- [56] A. Yamanaka, K. McReynolds, P.W. Voorhees, Phase field crystal simulation of grain boundary motion, grain rotation and dislocation reactions in a bcc bicrystal, *Acta Materialia* 133 (2017) 160-171.
- [57] D.A. Porter, K.E. Easterling, M. Sherif, *Phase Transformations in Metals and Alloys*, (Revised Reprint), CRC press 2009.
- [58] A.K. da Silva, R.D. Kamachali, D. Ponge, B. Gault, J. Neugebauer, D. Raabe, Thermodynamics of grain boundary segregation, interfacial spinodal and their relevance for nucleation during solid-solid phase transitions, *Acta Materialia* 168 (2019) 109--120.
- [59] J.W. Cahn, J.E. Hilliard, Free energy of a nonuniform system. I. Interfacial free energy, *The Journal of chemical physics* 28(2) (1958) 258-267.
- [60] V. Grolier, R. Schmid-Fetzer, Experimental study of Au-Pt-Sn phase equilibria and thermodynamic assessment of the Au-Pt and Au-Pt-Sn systems, *Journal of Electronic Materials* 37(3) (2008) 264-278.

- [61] A.T. Dinsdale, SGTE data for pure elements, *Calphad* 15(4) (1991) 317-425.
- [62] F. Abdeljawad, P. Lu, N. Argibay, B.G. Clark, B.L. Boyce, S.M. Foiles, Grain boundary segregation in immiscible nanocrystalline alloys, *Acta Materialia* 126 (2017) 528-539.
- [63] C. O'Brien, C. Barr, P. Price, K. Hattar, S. Foiles, Grain boundary phase transformations in PtAu and relevance to thermal stabilization of bulk nanocrystalline metals, *Journal of Materials Science* 53(4) (2018) 2911-2927.
- [64] D. MacLean, *Grain boundaries in metals*, 1957.
- [65] A.K. Da Silva, D. Ponge, Z. Peng, G. Inden, Y. Lu, A. Breen, B. Gault, D. Raabe, Phase nucleation through confined spinodal fluctuations at crystal defects evidenced in Fe-Mn alloys, *Nature communications* 9(1) (2018) 1137.
- [66] M. Kuzmina, D. Ponge, D. Raabe, Grain boundary segregation engineering and austenite reversion turn embrittlement into toughness: example of a 9 wt.% medium Mn steel, *Acta Materialia* 86 (2015) 182-192.
- [67] D. Raabe, S. Sandlöbes, J. Millán, D. Ponge, H. Assadi, M. Herbig, P.-P. Choi, Segregation engineering enables nanoscale martensite to austenite phase transformation at grain boundaries: a pathway to ductile martensite, *Acta Materialia* 61(16) (2013) 6132-6152.
- [68] X. Zhou, X.-x. Yu, T. Kaub, R.L. Martens, G.B. Thompson, Grain boundary specific segregation in nanocrystalline Fe (Cr), *Scientific reports* 6 (2016) 34642.
- [69] H. Aaron, G. Bolling, Free volume as a criterion for grain boundary models, *Surface Science* 31 (1972) 27-49.
- [70] L. Shvindlerman, G. Gottstein, V. Ivanov, D. Molodov, D. Kolesnikov, W. Łojkowski, Grain boundary excess free volume—direct thermodynamic measurement, *Journal of materials science* 41(23) (2006) 7725-7729.
- [71] E.-M. Steyskal, B. Oberdorfer, W. Sprengel, M. Zehetbauer, R. Pippan, R. Wüschum, Direct experimental determination of grain boundary excess volume in metals, *Physical review letters* 108(5) (2012) 055504.
- [72] V. Ivanov, D.A. Molodov, L.S. Shvindlerman, G. Gottstein, D. Kolesnikov, W. Łojkowski, Excess Free Volume of High Angle Grain Boundaries in Aluminium, *Materials science forum*, Trans Tech Publ, 2006, pp. 1557-1562.
- [73] M.A. Tschopp, G. Tucker, D. McDowell, Structure and free volume of $\langle 110 \rangle$ symmetric tilt grain boundaries with the E structural unit, *Acta materialia* 55(11) (2007) 3959-3969.
- [74] A. Seki, D.N. Seidman, Y. Oh, S. Foiles, Monte Carlo simulations of segregation at [001] twist boundaries in a Pt (Au) alloy—I. Results, *Acta metallurgica et materialia* 39(12) (1991) 3167-3177.

- [75] A. Seki, D.N. Seidman, Y. Oh, S. Foiles, Monte Carlo simulations of segregation at [001] twist boundaries in a Pt (Au) alloy—II. Discussion, *Acta metallurgica et materialia* 39(12) (1991) 3179-3185.
- [76] D.N. Seidman, Solute-atom segregation at internal interfaces on an atomic scale: atom-probe experiments and computer simulations, *Materials Science and Engineering: A* 137 (1991) 57-67.
- [77] F.R. De Boer, W. Mattens, R. Boom, A. Miedema, A. Niessen, *Cohesion in metals*, (1988).